J. Bangladesh Acad. Sci. 50(2); 215–232: June 2026 DOI: https://doi.org/10.3329/jbas.v50i2.90654

Journal of Bangladesh Academy of Sciences

Journal homepage: http://www.bas.org.bd/publications/jbas.html

Research Article

Silver nanoparticles decorated mesoporous-carbon/polyaniline nanocomposite based electrochemical sensor for dopamine detection

S Ahammed, S Shaha, S Razia[1], M A Rahaman, U Salma, and Md A Rashed[*]

Department of Chemistry, Faculty of Science, Mawlana Bhashani Science and Technology University, Santosh, Tangail 1902, Bangladesh

ARTICLE INFO

Article History

Received: 01 March 2026
Revised: 26 April 2026
Accepted: 29 April 2026

Keywords: AgNPs; Meso-C; Polyaniline; Biomolecule; DPV; Amperometry.

ABSTRACT

Dopamine (DA) is a key neurotransmitter in both the brain and the body, playing a significant role in a wide range of physiological functions. However, the presence of abnormal DA levels in the body is correlated with various health conditions. Thus, for the quantification and monitoring of DA, inventing a specific and sensitive detection method is a pressing need. In the present study, an Ag/Meso-C/Polyaniline (PAni) nanocomposite is deposited over the glassy carbon electrode (GCE) to design a highly efficient DA electrochemcial sensor. The electrocatalyst was synthesized via a facile ultrasonication and followed by photo-reduction. Then, sophisticated analytical techniques were applied to investigate its structural and morphological properties. Finally, the electrochemical performance of the Ag/Meso-C/PAni nanocomposite modified electrode was evaluated by using well-known electrochemical techniques. Obtained results demonstrated high sensitivity, which was estimated to be 0.228 μA μM^{-1} cm^{-2} (for differential pulse voltammetry, DPV) and 0.166 μA μM^{-1} cm^{-2} (for amperometry). This sensor also exhibits strong selective capability in the presence of common organic and inorganic species. Finally, the successful recovery analysis was conducted in the presence of a pharmaceutical formulation and blood serum.

Introduction

Human life largely depends on biomolecules, which are crucial for numerous biological functions involving growth, reproduction, and survival. Due to the growing imbalance in the natural metabolism of the human body, biomolecule analysis has become significant in modern times (Mahanthappa et al., 2022). The hypothalamic part of the human central nervous system generates DA, commonly referred to as 2-(3, 4-dihydroxyphenyl) ethylamine, a neurohormone with multiple functions in learning, memory, and emotion (Arpitha and Kumara, 2024).

An important neurotransmitter, DA can impact the central cognitive, hormonal, cardiovascular, and renal systems in mammals (Anuar et al., 2020). The primary function of DA is to transfer signals from the brain to other organs and areas of the body (Gaidukevic et al., 2022).

The range of DA level in human blood is 0.01–1.0 μM (Balkourani et al., 2023). Severe depression, addiction, schizophrenia, and illnesses, including Alzheimer's, Parkinson's, and Huntington's disease, can all result from an unbalanced DA concentration in the human brain (Mahanthappa et al., 2022;

Anuar et al., 2020). Therefore, a rapid, sensitive, and selective detection technique is needed to determine DA concentration in the human body.

[*]Corresponding author:<rashedlizon@gmail.com; abu.rashed@mbstu.ac.bd>

[1]*Department of Chemistry, Faculty of Applied Science and Humanities, Rajshahi University of Engineering and Technology, Rajshahi 6204, Bangladesh*

Conventional analytical methods such as High-Performance Liquid Chromatography (HPLC) (Mahanthappa et al., 2022; Zhang and Zheng,, 2019), UV-visible spectroscopy (Meenakshi et al., 2016; Joshi et al., 2016), Chemiluminescence (Joshi et al., 2016; Zhou et al., 2020), colorimetry method (Zhang and Zheng, 2019), fluorimetry (Zhang and Zheng, 2019; Meenakshi et al., 2016), flow injection analysis (Zhang and Zheng, 2019), and electrophoresis (Meenakshi et al., 2016) are available. But those conventional techniques are complex, time-consuming, and require expensive equipment (Zhang and Zheng, 2019). Those conventional methods can be replaced with specific, highly sensitive, and cost-effective electrochemical techniques (Nayak et al., 2020).

Electrochemical techniques can easily detect DA as it is an electroactive biomolecule. (Zhang and Zheng, 2019). However, in real physiological environments, interferences, such as ascorbic acid (AA) and uric acid (UA), inhibit the electroanalysis of DA, because of similar oxidation potential generating overlapping oxidation peaks, and second, at the electrode surface, oxidized DA undergoes reoxidation after being reduced by non-oxidized AA (Jiang et al., 2016). Therefore, it is highly desirable to investigate sensor electrodes based on nanomaterials that enhance catalytic performance (Liu et al., 2019). Due to the rapid advancement of nanotechnology, bare carbon electrodes have been modified with a variety of nanomaterials to improve DA sensing performance. Accordingly, nanomaterials, such as metallic nanoparticles, bimetallic alloys, metal oxide nanostructures, conducting polymers, and carbon-based materials and their hybrid composites, have been applied to develop electrochemical sensors for the selective detection of DA. Over the last two decades, conducting polymers like polypyrrole (PPy), polythiophene (Pth), and polyaniline (PAni) have received plenty of interest due to their potential applications in sensor research (Massoumi et al., 2013). One of the notable properties of conducting polymers is that, with the unique combination of doping and dopants, their electrical properties may be controlled throughout a broad range, from insulating to metallic (Massoumi et al., 2013; Wu et al., 2012; Rashed et al., 2022). Due to their π-conjugation system, conducting polymers offer a large specific surface area, thereby enhancing electron transfer (Bonyadi et al., 2020). Among conducting polymers, PAni is measured as the most promising candidate for sensor applications (Massoumi et al., 2013; Shin et al., 2017; Li et al., 2021). In contrast, the main drawbacks of using PAni are its inadequate electrical conductivity.

Novel metal nanoparticles like silver (Ag), platinum (Pt), and gold (Au) have drawn a lot of attention because of their extraordinary electrical conductivity, chemical stability, electrocatalytic ability (Massoumi et al., 2013). Owing to their rapid electron transfer, high catalytic efficiency, and superior biocompatibility, silver nanoparticles (AgNPs) have been widely employed in the development of biosensors (Zhang and Zheng, 2019). A certain drawback of using AgNPs in electrochemical sensor applications is their inherent aggregation. To prevent this, AgNPs are often disseminated into a conducting support matrix for practical applications (Liu et al., 2019). Due to their low-cost, high surface area, and excellent conductivity, carbon nanomaterials such as mesoporous carbon (Meso-C) are promising candidates for use as a support matrix. Taking advantage of AgNPs, Meso-C, and PAni, we introduce an electrochemical DA biosensor in this study. Previously, a DA electrochemical sensor has been introduced using Pt-Ag/graphene based nanocomposite, where a strong reducing agent hydrazine hydrate was used for the in-situ formation of Pt and AgNPs over the graphene surface, which makes the synthesis process complex and causes harm from environment (Anwar et al., 2020). In addition, D. Sangamithirai et al., reported Poly (o-anisidine)/Ag nanocomposite modified GC for DA sensing. Poly (o-anisidine) (POA) is a PAni derivative, which is biocompatible and dissolves in common organic solvents. However, POA has limitations in sensor applications due to its poor sensitivity and selectivity, and interference from other species. Though this

reported study shows a lower detection limit, the oxidation peak appears at a relatively higher overpotential. Moreover, this study discusses only the sensing properties (sensitivity and LOD). The catalytic investigation, reaction mechanism, interference study, real sample analysis were not demonstrated in this study (Sangamithirai et al., 2017).

In contrast, the present study avoids complex synthesis procedures, instead demonstrates a facile and straightforward synthesis route to fabricate the Ag@MesoC/PAni ternary nanocomposite. The structural and morphological features of the as-fabricated nanocomposite were elucidated through various advanced analytical techniques. Furthermore, its catalytic and sensing capabilities were systematically investigated via established electrochemical methods. The modified electrode exhibited superior selectivity toward DA in the presence of various organic and inorganic interfering species. Furthermore, the sensor was magnificently applied to real-sample analysis**,** yielding satisfactory recoveries in pharmaceutical and human serum matrices. Notably, this work represents the first report on the development of an electrochemical DA sensor based on an Ag@MesoC/PAni ternary nanocomposite.

Experimental

Materials

Analytical-grade chemicals and reagents were employed exactly as supplied, without additional purification. $AgNO_3$ salt, mesoporous carbon, 5 wt% Nafion Solution, and PAni were acquiredfrom Sigma-Aldrich (USA) in order to fabricate the sensor electrode. DA, the test analyte, was purchased from TCI, Japan. In order to maintain the pH of the solution 0.1 M phosphate buffer solution (PBS) was prepared by adding the required amount of $Na_2HPO_4.2H_2O$ and $NaH_2PO_4.2H_2O$ salts. 0.1 M NaOH and 0.1 M HCl were added to adjust the pH value of the synthesized PBS. The aforementioned chemicals, including 4-aminophenol (4-AP), urea, glucose, thiourea, ascorbic acid (AA), fructose, oxalic acid (OA), and paracetamol (PAR), were received from Merck, India. Throughout the experiment, fresh solutions were prepared every day using deionised water (DI-water).

Synthesis of Ag@Meso-C/PAni nanocomposite

A 2-step synthesis route was used to develop the ternary nanocomposite. First, 90 mL of DI-water-ethanol (50:50) was mixed with 0.94 g of PAni and stirred for 30 min with a magnetic stirrer. Following the addition of 0.05 g of Meso-C to the above suspension and sonicated for an hour at room temperature. Finally, the dropwise addition of the calculated amount of $AgNO_3$ (dissolved in DI-water) solution and 1.0 mL of CH_3OH to the Meso-C/PAni suspension. The Ag salt-doped Meso-C/PAni suspension was photo-irradiated for 20 hours using a Philips Hg lamp with an intensity of 2.0 mW cm^{-2} at 350 nm. The finished product was then dried overnight at 90 °C in an oven after being repeatedly rinsed with a DI-H_2O and CH_3OH mixture (80:20) to obtain 1 wt% AgNPs@5 wt% Meso-C/94 wt% PAni.

Characterization of the electro-catalyst Ag@Meso-C/PAni

The surface morphologies and microstructural characteristics of the as- prepared nanocomposite have been evaluated using sophisticated spectroscopic and microscopic equipment, including X-ray photoelectron spectroscopy (XPS), field emission scanning electron microscopy (FE-SEM), and Transmission electron microscopy (TEM). The structural properties (chemical environment and elemental composition) of the as-fabricated nanocomposite were demonstrated using a XPS K-ALPHA spectrometer (Thermo Fisher, USA). XPS fine scan deconvolution was carried out using open-source XPS PEAK41 software with a linear background. Surface morphology of the as-synthesized nanocomposite was studied with TEM and FE-SEM

microanalyzer. A JEOL JEM-2100 F-UHF instrument coupled with 1k-CCD camera and 200 kV acceleration voltage, and with a Gatan GIF 200 energy filter, was employed for TEM, and HR-TEM (high-resolution TEM) image recording. The morphological features and elemental composition of the fabricated nanocomposite were characterized using a JEOL-6300F scanning electron microscope (operating at 5 kV) equipped with an energy-dispersive X-ray spectroscopy (EDS) system.

Sensor Fabrication and Electrochemical Characterization

A glassy carbon electrode (GCE) with an inner diameter of 3.0 mm was purchased from ALS, BAS Inc. Japan for use as the working electrode. To get a mirror-like surface, GCE was progressively polished multiple times using 1.0, 0.3, and 0.05 µm alumina paste before surface modification. Then, the polished GC electrode was rinsed with ethanol and DI-water, followed by ultrasonication for 30 min in an ultrasonic bath using ethanol and DI-water. After that, a nitrogen stream was used to completely dry the electrode.

Then, the electrode modifier was prepared by taking 10 mg of the as-fabricated nanocomposite, which was dispersed in 900 µL of isopropanol and 100 µL of 5 wt% Nafion solution by using a vortex mixture followed by ultrasonication for an hour. To create the catalytically active layer, the freshly prepared 7.5 µL dispersion was applied dropwise (1.5 µL at a time) to the electrode surface and allowed to dry at room temperature. Finally, before the electrochemical analysis, the Ag@Meso-C/PAni/GCE electrode was dried in an oven at 60 °C for 30 min. All electrochemical investigations were conducted using a CHI-660E workstation (CH Instruments, USA) in a conventional three-electrode cell configuration. The setup comprised a spiral Pt wire counter electrode, a KCl-saturated Ag/AgCl reference electrode, and the Ag@Meso-C/PAni/GCE as the working electrode.

Results and Discussion

Characterization of nanocomposite

XPS analysis was conducted on the as-fabricated ternary nanocomposite in order to understand the chemical environment and elemental composition. The XPS survey scan spectrum for C 1s, O 1s, N 1s, and Ag 3d at their respective binding energy positions, confirming the successful formation of the ternary nanocomposite. The fine scan XPS spectra were calibrated with C 1s (284.5 eV) reference value with a linear background. Fig. 1(a–d) reveals the XPS fine scan deconvolved spectra. As per binding energies, C 1s splits into four distinguished peaks (Fig. 1(a)). Peaks at 284.5 eV for C-C and 285.6 eV, 286.9 eV could be ascribed to C-H, C–O, respectively (Chen et al., 2020). Finally, the peak at higher binding energy (288.1 eV) resulted for C=O. N 1s splits into two distinguished peaks at binding energies 398.1 eV and 399.3 eV (Fig. 1(b)), which could be attributed to nitrogen for imine structure and amine-like nitrogen atoms (NH), respectively (Li et al., 2016). The XPS fine scan spectra of O 1s (Fig. 1(c)) were deconvoluted with four distinguished peaks. Chemical states for O 1s were represented at 532.8 eV for C-O-C, and the peak attributed at 531.7eV is related to C=O (Briggs and Beamson, 1993). Another two low-intensity peaks located at 530.6 eV and 533.8 eV are attributed to the hydrated phase of metal nanoparticles and adsorption of H_2O from the surrounding or lattice oxygen attached on the catalyst surface, respectively (Rashed et al., 2022; Jackman et al., 2015). Finally, Fig. 1(d) represents Ag 3d fine-scan spectra, containing two main peaks at 367.7 eV and 373.8 eV binding energies, respectively to Ag $3d_{5/2}$ and Ag $3d_{3/2,}$ which indicates Ag is in a metallic state. The splitting of ~6 eV is due to the spin-orbit coupling (Ji et al., 2015).

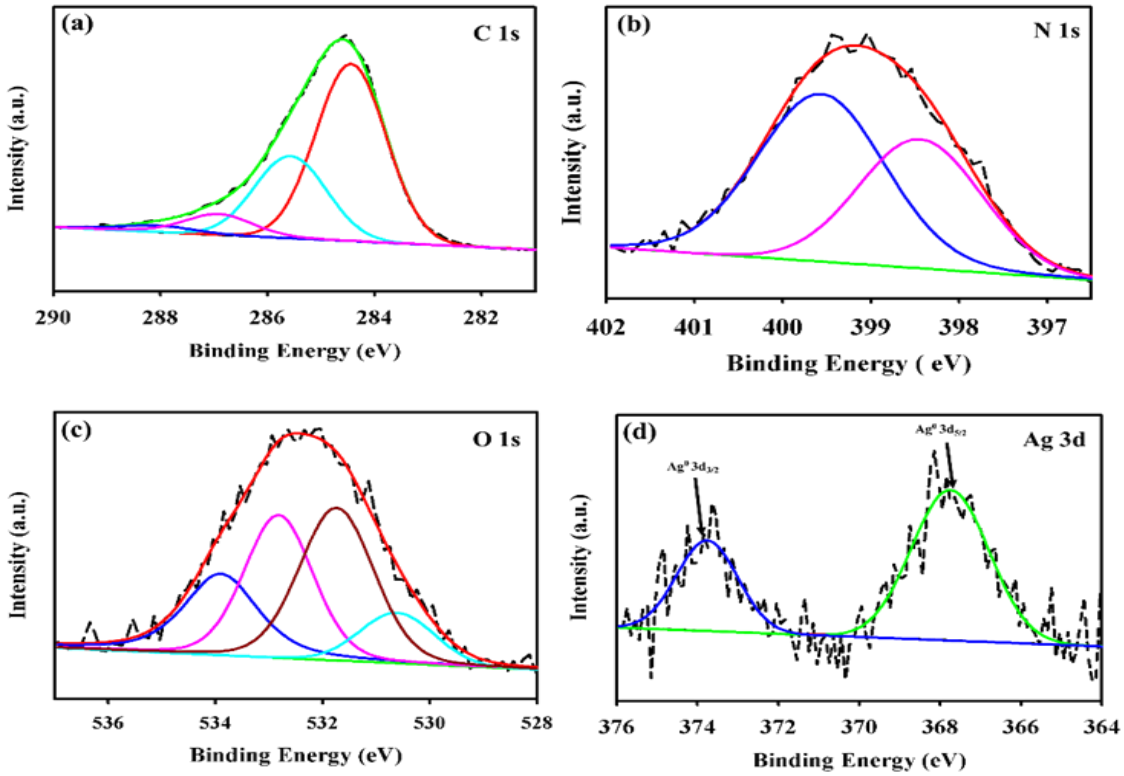

Fig. 1. XPS fine scan spectra of (a) C 1s, (b) N 1s, (c) O 1s, and (d) Ag 3d.

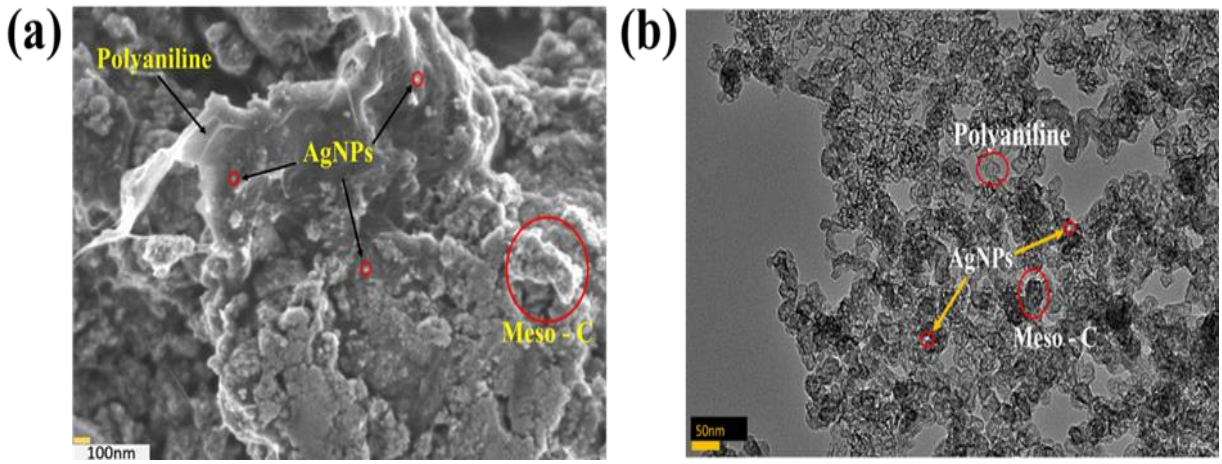

Fig. 2. (a)SEM and (b) TEM images of Ag@Meso-C/PAni nanocomposite.

Using SEM and TEM techniques, the morphological analysis of the as-synthesised nanocomposite was well justified. Fig. 2 (a) shows the SEM image of the Ag@Meso-C/PAni composite. The AgNPs are visible as white spots on the surface, indicating a homogeneous dispersion over the Meso-C/PAni matrix. The obtained results confirm the successful formation of the nanocomposite. Additionally, the successful doping of AgNPs on the Meso-C/PAni matrices is shown by the TEM image (Fig. 2(b)). The HR-TEM image of Ag@Meso-C/PAni TEM showed that the AgNPs (white dots) and Meso-c dopant were evenly distributed across the PAni nanostructure.

Table 1. The voltametric response concerning peak current and peak potential for DA redox at various working electrodes.

Electrodes	E_{pa} (V)	I_{pa} (uA)	E_{pc} (V)	I_{pc} (uA)	ΔE_p (V)
Ag@Meso-C/PAni/GCE	0.190	4.860	0.153	-1.228	0.037
Ag@Meso-C/GCE	0.187	4.138	0.132	-1.240	0.055
Meso-C/PAni/GCE	0.238	3.174	0.098	-1.455	0.14
Meso-C/GCE	0.201	3.091	0.122	-1.726	0.079
PAni/GCE	0.250	2.378	0.105	-0.620	0.145
GCE	0.222	1.258	0.148	-0.158	0.074

Electro-catalytic performance of DA on Ag@Meso-C/PAni/GCE modified electrode

The electro-catalytic efficiency of the as-fabricated nanocomposite modified GCE was assessed using Cyclic voltammetry (CV) and electrochemical impedance spectroscopy (EIS) concerning 0.15 mM of DA in a 0.1 M PBS (pH=7.0) electrolyte. As seen in Fig. 3(a), the voltammograms of PAni/GCE, Meso-C/GCE, Meso-C/PAni/GCE, Ag@Meso-C/GCE, and Ag@Meso-C/PAni/GCE were investigated in the presence of 0.15 mM DA, and the potential window was between -0.1 and +0.5 V, with a scan rate of 20 mV/s.

Under similar experimental conditions, Ag@Meso-C/PAni/GCE shows the maximum I_{pa} with a slightly lower potential value, whereas bare GCE displays a small I_{pa} with a relatively high potential value. The CV analysis shows that the redox peaks (ΔE_p) separate at 0.074 V and 0.037 V for the GCE and Ag@Meso-C/PAni/GCE electrodes, respectively (shown in Table 1). This suggests that the small ΔE_p value of Ag@Meso-C/PAni/GCE facilitates facile electron transfer. The I_{pa} of the Ag@Meso-C/PAni/GCE is 4.86 µA at 0.19 V, which is significantly higher than its counterparts. The bare GCE had a modest redox current peak, with an I_{pa} of about 1.258 µA at 0.22 V. These results show that the ternary nanocomposite shows a significantly greater catalytic activity towards DA electro-oxidation. The catalytic effectiveness of Ag@Meso-C/PAni towards DA oxidation has been further verified by an EIS investigation shown in Fig 3 (b). The EIS has advantages over other electrochemical methods in separating the solution impedance from slight interruption of electrode-solution interference events.

In the presence of 0.15 mM of DA in 0.1 M PBS (pH 7.0), EIS was conducted for the GCE, PAni/GCE, Meso-C/GCE, Meso-C/PAni/GCE, Ag@Meso-C/GCE, and Ag@Meso-C/PAni/GCE electrodes at a frequency of 10^5 Hz and an applied potential of 0.2 V. In the higher-frequency region, the smaller diameter of the semicircle revealed a lower charge transfer resistance (R_{ct}) at the surface-solution interface, which also demonstrated higher electrical conductivity (Balkourani et al., 2023). From the observed Nyquist plot, it was revealed that Ag@MesoC/PAni modified GC electrode shows the lower semicircle diameter in the higher frequency region, indicating the lowest R_{ct} value and highest electrical conductivity among the examined electrodes (Fig. 3(b)). The unmodified GCE shows a greater charge transfer resistance under the same experimental circumstances as the EIS investigation. This suggests that the bare electrode has poor catalytic activity and slow electron transfer kinetics.

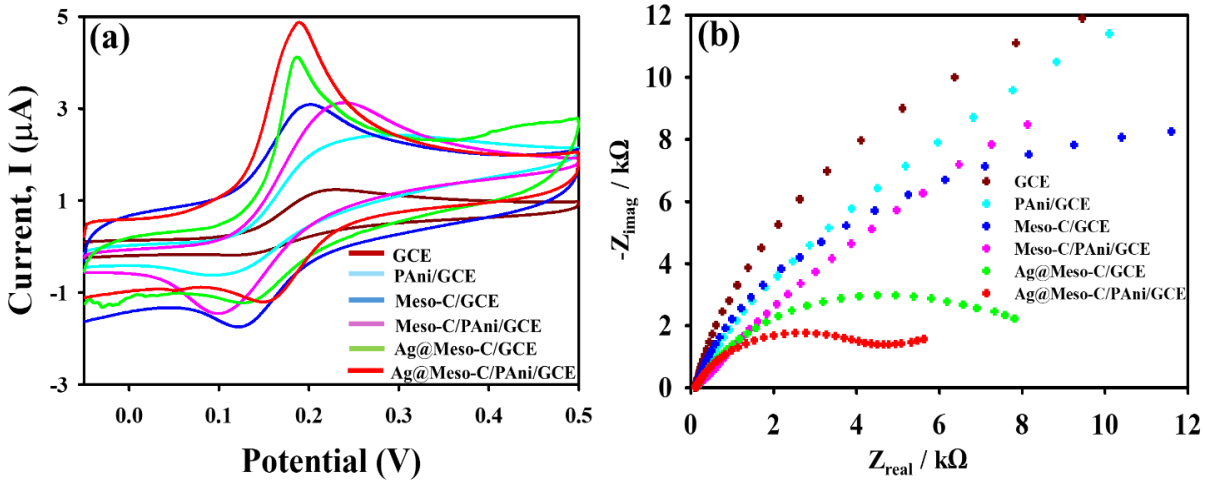

Fig. 3. (a) CV response at 0.15 mM of DA in 0.1 M PBS (pH= 7.0) at scan rate 20 mVs^{-1} (b) EIS Nyquist plot recorded in 0.1 M PBS (pH=7.0) containing 0.15 mM of DA at applied potential 0.2 V, 1 to10^5 Hz frequency range by using GCE, PAni/GCE, Meso-C/GCE, Meso-C/PAni/GCE, Ag@Meso-C/GCE, and Ag@Meso-C/PAni/GCE working electrode.

The strong catalytic efficiency of modified electrodes towards DA oxidation is likely caused by the wide surface area and good electrical conductivity of the nanocomposite. Particularly, network-like structure of PAni and Meso-C nanocomposites increases conductivity and provides a more appropriate surface for accommodation of AgNPs without aggregation. The synergistic interaction among AgNPs, Meso-C, and PAni would influence the electron transfer kinetics. It might help the electrochemical oxidation of DA and lead to enhanced electrochemical performance of modified electrodes (Ghanbari et al., 2019).

Effect of the electrolyte medium

Further investigation was conducted on how pH of the electrolyte (0.1 M PBS) affects electrochemical performance of the Ag@Meso-C/PAni/GC electrode towards DA electro-oxidation. In Fig. 4(a), differential pulse voltammograms (DPVs) of 0.10 mM DA were measured in 0.1 M PBS at pH variation between 6.0 to 9.0. The voltammogram indicates that peak current increases as pH values rise from 6.0 to 7.0, reaches its maximum, and then falls from 7.0 to 9.0, which is observed from Fig 4(b).

In addition, the oxidation peak potentials shifted towards a negative potential direction with increasing electrolyte pH. The reason is that oxidation process in influenced by higher pH levels, which undergoes a deprotonating step. The relationship between peak potential and electrolyte pH demonstrates linear correlation with a slope of 71 mV/pH (Fig 4 (c)). This is close to the Nernst value 59 mV. The determined slope value reveals that the electrocatalytic oxidation of DA comprises an equal contribution of protons and electrons **(**Li et al., 2021). The proposed DA electro-oxidation mechanism is shown in Scheme 1.

Kinetics study of the redox behavior of DA

The scan rate-dependent CVs were obtained by varying the scan rates from 5 to 200 mV/s in 0.1 M PBS (pH 7.0) containing 0.15 mM of DA to provide a concise explanation of the DA electrochemical reaction kinetics in Fig. 5 (a–c). Fig. 5(a) exemplifies that redox peak current steadily surges when the scan rate rises. A correlation exists between scan rate and peak potential shift; the oxidation and reduction peak potentials are shifted towards the positive and negative potential direction, indicating the process is irreversible in nature (Kenarkob and Pourghobadi, 2019).

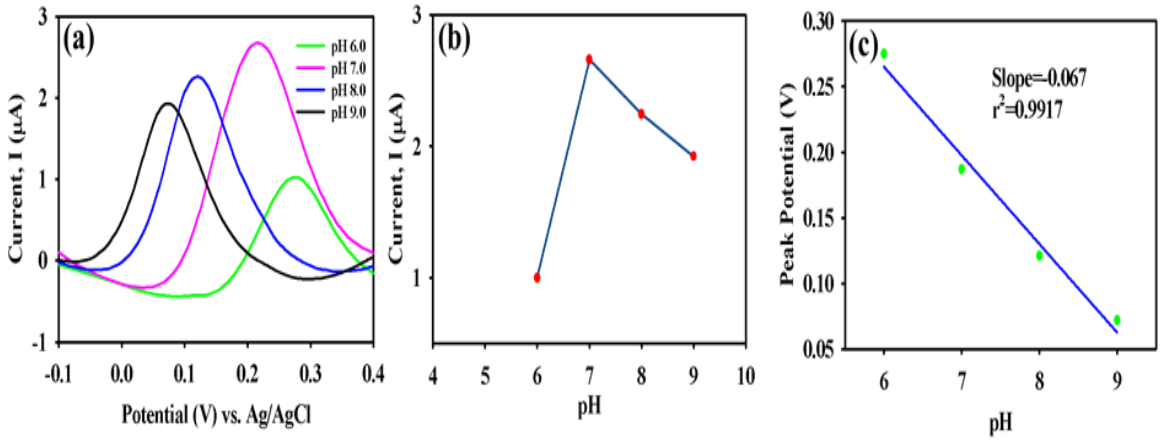

Fig. 4. (a) CV response of Ag@Meso-C/PAni/GCE modified nanocomposite for 0.15 mM DA in 0.1mM PBS with pH range 6.0 to 9.0 at a scan rate of 20 mV s^{-1}. (b) represented the relationship between peak current *vs.* pH, and (c) shows the regression plot of peak potential *vs.* pH.

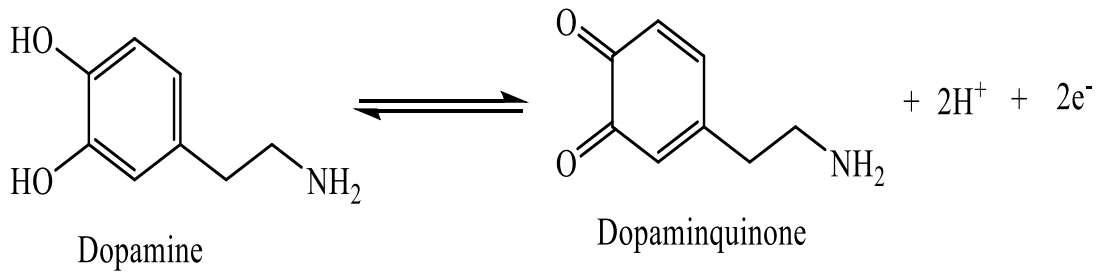

Scheme 1. Proposed mechanism of electrochemical oxidation of DA (Zhang and Zheng, 2019).

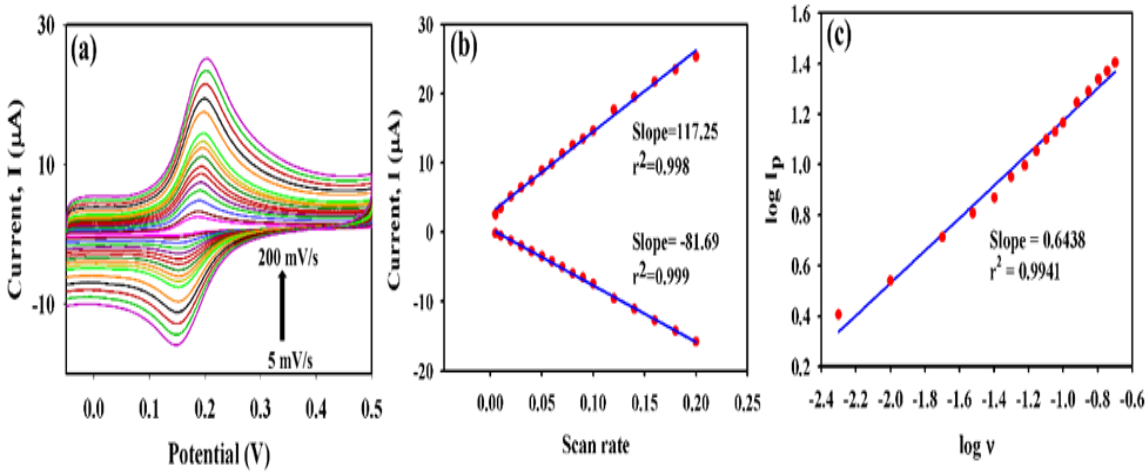

Fig. 5. (a) CV response recorded of Ag@Meso-C/PAni/GCE modified electrode for 0.15 mM DA in 0.1 mM PBS (pH=7) with varying scan rate 5-200 mV s^{-1}. (b) linear relationship between peak current vs. scan rate (v). (c) relationship between log of peak current vs. log scan rate.

A linear relationship between both I_{pa} and I_{pc} with scan rate as indicated by Eqs. (i) and (ii) (Fig. 5(b)), indicating the electrochemical redox reaction of DA follows a surface adsorption-controlled nature (Huang et al., 2014).

I_{pa} (μA) = 117.25 ν + 2.7874; r^2 = 0.998 (i)

I_{pc} (μA) = − 81.69ν + 0.4825; r^2 = 0.999 (ii)

Based on the slope values presented in Fig. 5(b), the slope of the oxidation peak is around 1.4 times greater than the slope of the reduction peak.

Moreover, Fig. 5(c) shows a slope value of 0.6438 for the correlation between log I_{pa} and log ν. According to the literature, electrochemical reaction follows diffusion-controlled kinetics when the slope values range from 0.2 to 0.6, whereas it should be adsorption-controlled kinetics when values between 0.75 and 1.0. A slope value of 0.60 to 0.75 indicates the mixed adsorption-diffusion control system (Jaiswal et al., 2017). The obtained slope value for the electro-oxidation reaction of DA at the Ag@Meso-C/PAni/GCE is 0.6438. Thus, it follows a mixed adsorption-diffusion-controlled kinetics mechanism.

Analytical performance of Ag@Meso- C/ PAni/ GCE towards DA detection

Electrochemical sensing capabilities of the designed Ag@Meso-C/PAni nanocomposite-modified GCE were evaluated using the sensitive Differential Pulse Voltammetry (DPV) method. For electrochemical sensor studies, DPV was selected over CV due to its greater sensitivity and higher resolution (Devaraj et al., 2013). As part of the analytical performance, the DA concentration was varied between 5.0 μM and 306.27 μM in a 0.1 M PBS (pH=7.0) solution, illustrated in Fig. 6(a). The I_{pa} gradually rises when the analyte is added successively. The availability of inherent free charge, which supports the identifying capability of DA towards Ag@Meso-C/PAni/GCE sensor, is related to the steady growth of I_{pa} (Rashed et al., 2021). However, when the analyte concentration increased, a small shift in the peak potential towards a more positive potential direction could be observed. This shifting seems to be a consequence of the saturated adsorption of the target analyte on the working electrode surface, or it may be linked to the by-products formation during the course of the reaction (Wanget al., 2011; Rahman et al., 2024; Majidi and Ghaderi, 2017).

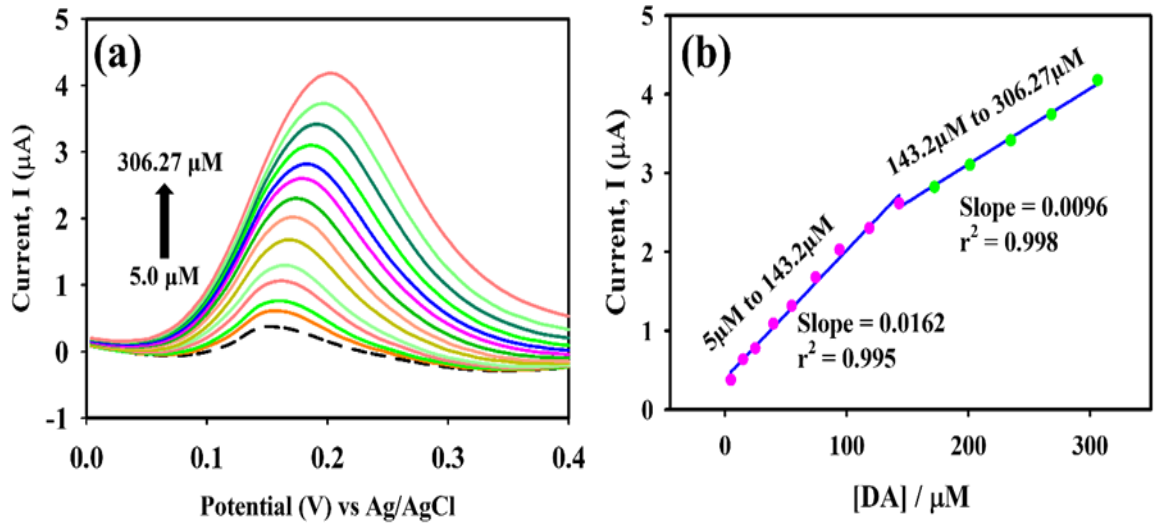

Fig. 6. (a) DPV response of Ag@Meso-C/PAni/GCE modified electrode for analytical performance involved varying the DA concentration within the range of 5 μM to 306.27 μM in a 0.1M PBS (pH=7.0). (b) depicts the linear relationship of current *vs.* concentration of DA.

The calibration plot of I_{pa} vs. [DA] is shown in Fig. 6(b). Two linear segments for DA over concentrations of 5 µM to 143.2 µM and 143.2 µM to 306.27 µM are identified. For the first linear range (5 µM to 143.2 µM) and the second linear range (143.2 µM to 306.27 µM), the linear regression equation was fitted in Eq. (iii) and Eq. (iv), respectively. The deviation of the calibration curve at higher concentrations may occur either due to the surface coverage or due to reaching saturation absorption.

$$y = 0.0162\ [DA / (\mu M)] + 0.39;\ r^2 = 0.995 \quad \text{(iii)}$$

$$y = 0.0096\ [DA / (\mu M)] + 1.19;\ r^2 = 0.998 \quad \text{(iv)}$$

The sensitivity was computed using the obtained slope value divided by the apparent surface area of the GC electrode (0.071 cm^2). For the first segment, the sensor sensitivity was estimated to be 0.228 µA $\mu M^{-1}\ cm^{-2}$, and for the second linear segment, it was estimated to be 0.135 µA $\mu M^{-1}\ cm^{-2}$. In addition, Eq. (v) was employed to calculate the limit of detection (LOD) (Faisal et al., 2025; Dhanavel, and Ravethy ., 2018).

$$LOD = \frac{3 \times S_b}{m}\ (S/N=3) \quad \text{(v)}$$

Here, "m" refers to the slope value (0.0162 and 0.0096, respectively), S_b (standard deviation) of seven blank DPV measurements in 0.1 M PBS (pH=7.0), where the value was found to be 0.0052 µA. The LOD was found to be 0.96 µM and 1.63 µM using Eq. (v).

The active nanocomposite modified GC towards DA sensing was further determined using amperometry, one of the most accurate and highly sensitive electrochemical processes. The pH of the supporting electrolyte and the amperometric working potential are vital for sensing the target analyte (Rashed et al., 2022). To optimise the working potential, amperometric investigations were conducted in various working potentials (0.30, 0.35, and 0.40 V) by successively injecting the analyte solution into 0.1 M PBS (pH=7.0) while constant stirring, as shown in Fig. 7(a).

The *I vs.* [DA] calibration curve in Fig. 7(b), from the regression coefficient (r^2) and the slope of those linear curves, the Ag@Meso-C/PAni modified electrode indicates its maximum sensing capabilities at a working potential of 0.35 V. Therefore, for further amperometric studies in DA electrochemical sensing, a working potential of 0.35 V was selected. An amperometric study was performed to ascertain a suitable pH level of the supporting electrolyte. As illustrated in Fig. 7(c), the pH of the PBS solution was increased from 5.0 to 8.0 while maintaining the working potential at 0.35V. Fig. 7(d) shows the linear response of the calibration curve for *I* vs. [DA]. A neutral pH (pH=7.0) demonstrated the maximum sensitivity when comparing the slope and r^2 values. So, a pH-7 was chosen for further amperometric analysis. Finally, the Ag@Meso-C/PAni sensor electrode was used to perform the electrochemical sensing using an amperometric technique by progressively injecting the DA solution into PBS while stirring continuously. During this process, DA is gradually added to 0.1 M of PBS in the concentration range of 5.0 µM to 369.10 µM by maintaining the previously optimized parameters (0.35 V working potential with pH-7 electrolyte medium), as illustrated in Fig. 7(e). In this instance, the sensitivity was computed based on.

By the current *vs.* [DA] curve (Fig. 7(f)), two linear segment was appeared at lower and higher concentration regimes. The sensitivity of the as-fabricated sensor is thus calculated to be 0.166 µA $\mu M^{-1}\ cm^{-2}$ for the first segment and 0.085 µA $\mu M^{-1}\ cm^{-2}$ for the second linear in that segment. According to the sensitivity data, both DPV and amperometric approaches show a considerable decrease in sensor sensitivity in the higher concentration region as compared to the lower one. This phenomenon could be attributed to the blocking of the electrode surface or poisoning of the catalytic surface by the formation of by-products.

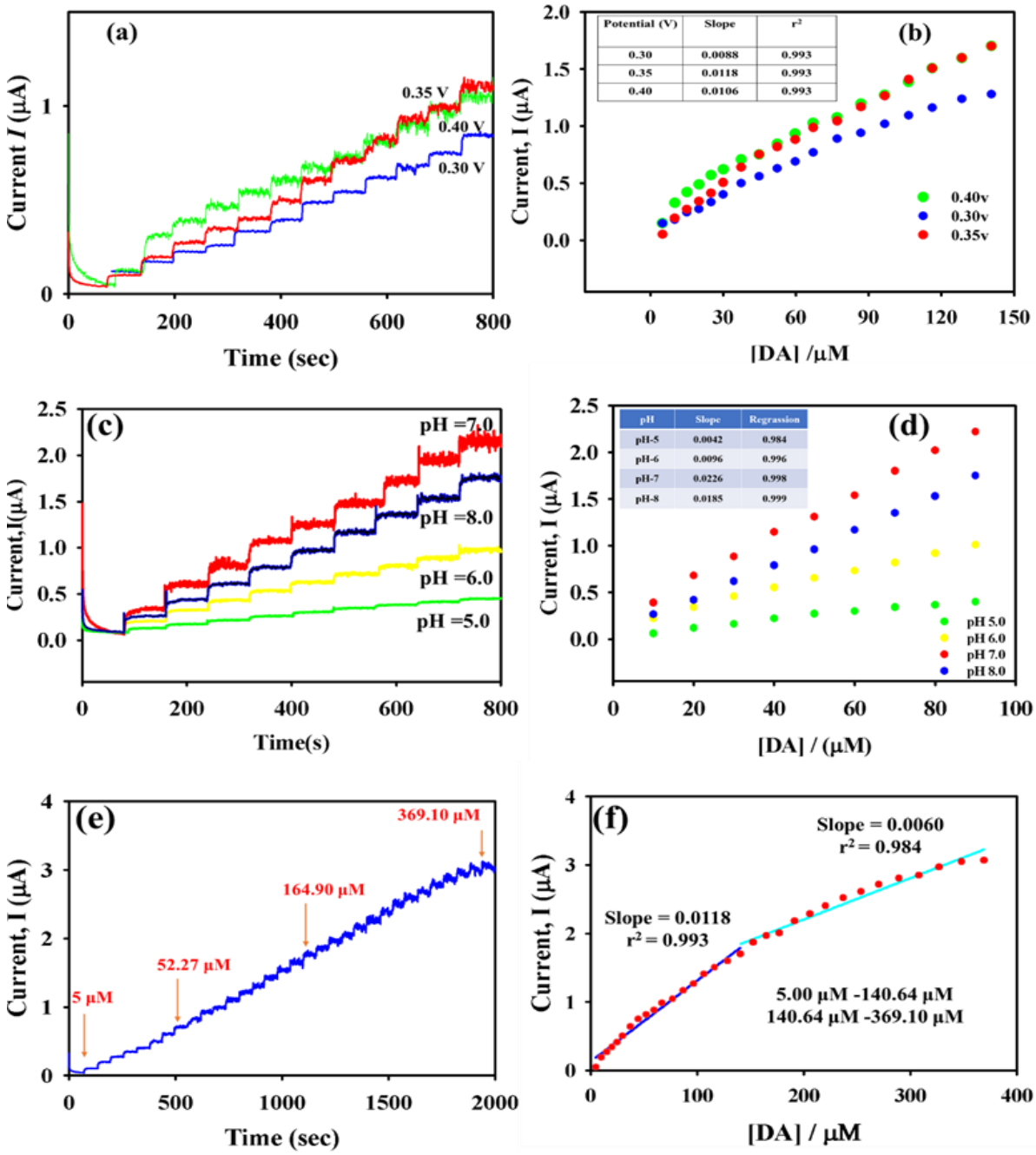

Fig. 7. (a) Amperometric response of the Ag@Meso-C/PAni/GCE nanocomposite in 0.1 M PBS (pH=7.0) solution in different working potentials (0.30 V, 0.35 V, and 0.40 V) upon the continuous addition of DA. (b) Calibration curve of current *vs.* [DA] at different working potentials. (c) Amperometric response of the Ag@Meso-C/PAni/GCE nanocomposite in 0.1 M PBS with pH range from 5.0 to 8.0 in working potential 0.35 V upon the continuous addition of DA. (d) Calibration curve of current *vs.* [DA] at different pH. (e) Amperometric (i-t) sensing investigation of Ag@Meso-C/PAni/GCE electrode by successive addition of DA in 0.1 M PBS (pH=7) at working potential 0.35 V. (f) current *vs*. [DA] calibration plot.

The LOD was found to be 1.340 µM and 2.60 µM, applying Eq. v. Table 2 demonstrates the comparison of the sensor performance in terms of detection range and LOD by this fabricated sensor with previously reported relevant sensor electrodes.

Thus, the newly created Ag@Meso-C/PAni sensor electrode showed comparable sensitivity, linear detection range (LDR), and LOD for the measurement of DA. Noteworthy that it also exhibited quick sensing capabilities.

Operational Stability, Reproducibility, and Selectivity

A vital part of verifying the capability of the sensor for practical application is the selectivity or interference test. Thus, amperometric technique was used to examine the selectivity of our proposed sensor (Fig. 8(a)).

This research systematically analysed the influence of potential interference from common interfering species on the detection of DA under optimized conditions. The interfering species, like urea, ascorbic acid (AA), glucose, fructose, thiourea, oxalic acid (OA), 4-aminophenol, and paracetamol were applied at thirty times higher concentration than the target DA. Notably, during the amperometric analysis, the DA concentration was set at 10 µM. When DA was added to a 0.1 M PBS solution under optimal amperometric conditions, an immediate current response was seen. However, when interfering organic species were added one after the other, no or insignificant current response was found.

Table 2. Comparison of sensor performance with the previously reported relevant sensor electrodes.

Electrode	Method	Linear range (µM)	LOD (µM)	Reference
Ag-doped PAni nanocomposites/GCE	Amperometric	10.0-90.0	1.9	(Paulraj et. al., 2020)
Chitosan–graphene/GCE	DPV	1000–24000	1000	(Han, 2010)
PAni-NF/Pt	DPV	2.0 – 10 and 40 – 400	0.6	(Bagherzadeh et al., 2015)
PAni-GO/GCE	DPV	2-18	0.5	(Manivel, 2013)
AuNPs@PAni	DPV	10–1700	5	(Yang et al., 2012)
PAni-MWCNTs	-	50–385	38	(Chang et al., 2019)
Au/Gr-AuAg	SW	10–100	2.16	(Pruneanu et al., 2015)
MoS_2PAni/rGO/GCE	DPV	5.0–500	0.70	(Li, 2019)
Ag@MesoC/ PAni/GCE	Amp	5.00 – 140.64	1.32	This Work
		140.64 –369.10	2.60	
	DPV	5.00 – 143.20	0.96	
		143.20 –306.27	1.63	

PAni= Polyaniline; GCE= Glassy Carbon Electrode; PAni-NF = Polyaniline Nanofibers; CS= Chitosan; AuNPs = Gold Nano Particles; MWCNTs = Multi-Walled Carbon Nanotubes; rGO = reduced graphene oxide; Meso-C = Mesoporous-C.

The oxidation potential of those interfering molecules is different from that of the oxidation potential of the DA, which may be the cause of the selectivity of the as-fabricated sensor in this experimental condition. Therefore, it may be anticipated that the sensor now under development will be able to determine DA in practical samples in a selective manner. In order to evaluate the sensor electrode stability, a prolonged amperometric response was recorded under optimized conditions (working potential 0.35V and pH-7) (Fig. 8(b)). The amperometric run was conducted for 120 min from the initial injection of 15 µM DA in the reaction vessel. The results exhibited after 120 min of continuous running showed a ca. 19 % decline in current intensity from the initial value. This result shows that even after prolonged electrolysis, the studied sensor displays good operational stability. Moreover, the stability test of the as-febricated sensor was conducted using 20 repeated cycles (Fig. 8(c)) using 0.10 mM of DA at 0.1 M PBS. From I_{pa} *vs*. no of cycles diagram, it is revealed that there is no significant changes of current intensity to demonstrate exceptional cyclic stability of the as-fabricated sensor electrode towards DA detection. Additionally, voltammograms of four distinct modified electrodes were taken under identical testing conditions in order to test the reproducibility of the analysed sensor electrode (Fig. 8(c)). The bar diagram of current response *vs*. no of tested electrode shown in Fig. 8(d). The %RSD of the current response was found to be 3.41%, depending on the DPV response. From the above obtained results, the designed sensor has demonstrated significant selectivity, stability, and reproducibility. Finally, the results of this study could lead the way for the development of innovative electrochemical sensors for targeted molecules.

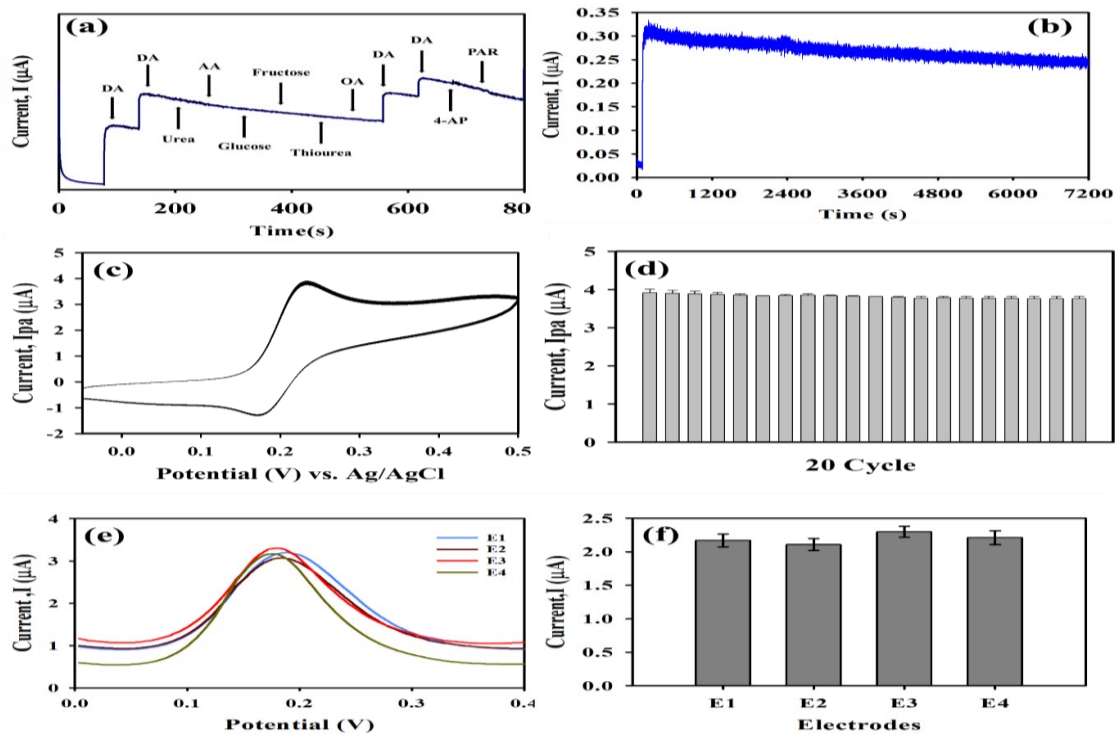

Fig. 8. (a)Selectivity test of Ag@Meso-C/PAni/GCE at a thirty-times higher concentration of urea, AA, glucose, fructose, thiourea, OA, 4-AP, and PAR, interfering species than the target DA in 0.35 working potential. (b) Amperommetric response in 0.35V working potential in 0.1M PBS (pH=7.0), after initially injecting 0.15 mM of DA at 120 minutes of prolonged electrolysis. (c) CV response of 20 repeated cycles at 0.1 mM DA at 0.1 M PBS (pH-7), scan rate 20 mVs^{-1}. (d) bar diagram of current vs. repeated cycles. (e) Reproducibility test done by DPV of four different Ag@Meso-C/PAni/GCE electrodes for 0.15 mM DA in 0.1mM PBS (pH=7). (f) bar diagram between current *vs*. number of electrodes.

Real sample analysis

The validation of the fabricated sensor electrode towards practical application was evaluated using a commercially available DA formulation (D-Dopamine IV Injection, Drug International Ltd., Bangladesh). The recovery test was conducted using the standard addition method at three different concentrations. The calculated recovery percentages shown in Table 3 varied from 95.5 to 99.2, demonstrating the outstanding accuracy, reliability, and tolerable matrix interference of the sensor. Furthermore, to validate the sensor in a complex biological matrix, the sensor performance was investigated in the presence of human blood serum as a real sample. Blood was collected from the university medical center and was then diluted ten times with supporting electrolyte (0.1 M PBS pH 7.0) to reduce the matrix complexity, and recovery analysis was conducted by the well-known standard addition method. A known concentration of target DA was injected into the diluted blood serum samples, whereas the presence of DA in the real sample seems to be negligible. To evaluate the accuracy of the sensor, three individual DPV measurements were carried out with three different concentrations. Table 4 displays an excellent recovery range from 96.67% to 101.0%, and they were accompanied by acceptable %RSD values indicating good accuracy and precision.

These results highlight ability of the sensor to detect DA in complex matrices, illustrating its reliability for practical clinical and pharmaceutical applications.

Conclusion

A two-step synthesis approach was successfully used to precisely combine AgNPs, Meso-C nanomaterials, and PAni biopolymer to develop a novel electrocatalyst. The Ag@Meso–C/PAni modified sensor electrode was developed by drop-casting this nanocomposite over a GCE surface. This electrode was then used for the electrochemical analysis of DA. Compared to Ag@Meso-C/GCE, Meso-C/PAni/GCE, Meso-C/GCE, PAni/GCE, and the unmodified GCE, the as-synthesised Ag@Meso-C/PAni/GCE nanocomposite exhibits higher electrocatalytic activity towards DA. Because of the synergistic interactions among its constituents and the momentous rise in the exposed surface area of the electrocatalyst, the ternary nanocomposite displayed exceptional catalytic and sensing performance. Kinetic studies showed that the electrooxidation of DA followed a mixed adsorption-diffusion-controlled kinetics mechanism. The examined sensor exhibits high sensitivity, which was calculated as 0.228 $\mu A \mu M^{-1} cm^{-2}$ & 0.135 $\mu A \mu M^{-1} cm^{-2}$ (for DPV), and 0.166 $\mu A \mu M^{-1} cm^{-2}$ and 0.085 $\mu A \mu M^{-1} cm^{-2}$ (for Amperometry). The sensor electrode exhibited strong anti-interference capabilities in the presence of common interfering species. This Ag/Meso-C/PAni nanocomposite exhibited promising performance as an electrocatalyst for sensitive and selective DA determination.

Table 3. DA recovery analysis in commercial D-Dopamine using DPV technique as real sample by standard addition method.

Sample	Sample (mM)	Standard DA added (mM)	Total (mM)	Found (µM)	Recovery (%)	Average Recovery (%)	% RSD
D-Dopamine (Drug International Ltd.)	0.04	0.06	0.1	0.093	93.00	96.00	3.750
				0.095	95.00		
				0.100	100.00		
	0.04	0.16	0.2	0.190	95.00	95.50	0.906
				0.193	96.50		
				0.190	95.00		
	0.04	0.26	0.3	0.307	102.30	99.22	4.850
				0.281	93.67		
				0.305	101.67		

Table 4. DPV recovery test of DA in human blood serum as real samples using standard addition method.

Sample	Standard DA added (mM)	Found (mM)	Recovery (%)	Average Recovery (%)	% RSD
Blood serum	0.10	0.095	95.0	96.67	2.151
		0.099	99.0		
		0.096	96.0		
	0.15	0.148	98.67	97.78	1.48
		0.145	96.66		
		0.147	98.0		
	0.20	0.205	102.5	101.0	2.09
		0.202	101.0		
		0.199	99.5		

Acknowledgment

The authors acknowledge Grants for Advanced Research in Education (GARE), Bangladesh Bureau of Educational Information & Statistics (BANBEIS) (Project ID: PS20232552), Ministry of Education, Bangladesh.

Author contribution

S. Ahammed: Writing original draft, Methodology, Investigation, Formal analysis, Software; S. Shaha: Writing original draft, Methodology, Investigation, Formal analysis; S. Raiza: Investigation, Formal analysis, Software; M. A. Rahaman: Writing review & editing, Validation; Umme Salma: Writing review & editing, Formal analysis; Md. A. Rashed: Writing review & editing, Validation, Supervision, Methodology, Conceptualization, Fund acquisition.

Conflict of interest

The authors declare there is no conflict of interest.

References

Anuar NS, Basirun WJ, Shalauddin M, and Akhter S. A dopamine electrochemical sensor based on a platinum-silver graphene nanocomposite modified electrode. *RSC Adv*. 2020; 10(29): 17336–17344.

Arpitha SB and Kumara Swamy BE. Synthesis and electrochemial performances of CuO/MgO nanocomposite as a sensing platform for dopamine. *Microchem J*. 2024; 206: 111584.

Bagherzadeh M, Mozaffari SA, and Momeni M. Fabrication and electrochemical characterization of dopamine-sensing electrode based on modified graphene nanosheets. *Anal. Methods*. 2015; 7(21): 9317–9323.

Balkourani G, Brouzgou A, and Tsiakaras P. A review on recent advancements in electrochemical detection of dopamine using carbonaceous nanomaterials. Carbon N Y. 2023; 213.

Bonyadi S, Ghanbari K, and Ghiasi M. All-electrochemical synthesis of a three-dimensional mesoporous polymeric g-C3N4/PANI/CdO nanocomposite and its application as a novel sensor for the simultaneous determination of epinephrine, paracetamol, mefenamic acid, and ciprofloxacin. *New J. Chem*. 2020; 44(8): 3412–3424.

Briggs D and Beamson G. XPS Studies of the Oxygen 1s and 2s Levels in a Wide Range of Functional Polymers. *Anal Chem*. 1993; 65(11): 1517–1523.

Chang YH, Woi PM, and Alias Y. The selective

electrochemical detection of dopamine in the presence of ascorbic acid and uric acid using electro-polymerised-β-cyclodextrin incorporated f-MWCNTs/polyaniline modified glassy carbon electrode. *Microchem. J*. 2019; 148: 322–330.

Chen X, Wang X, and Fang D. A review on C1s XPS-spectra for some kinds of carbon materials. *Fuller. Nanotub Carbon Nanostruct*. 2020; 28: 1048–1058.

Devaraj M, Deivasigamani RK, and Jayadevan S. Controlled growth and molecular self-assembly of Au nanoparticles to Au nanochains: Application towards enhancement for the electrochemical determination of paracetamol. *Anal. Methods*. 2013; 5(14): 3503–3515.

Dhanavel S, Revathy TA, Padmanaban A, Narayanan V, and Stephen A. Highly efficient catalytic reduction and electrochemical sensing of hazardous 4-nitrophenol using chitosan/rGO/palladium nanocomposite. *J. Mater. Sci. Mater Electron.* 2018; 29(16): 14093–14104.

Faisal MM, Ali SR, Hussain G, Autieri C, Sánchez EM, Castro AT, and Sanal KC. Tungsten carbide as an electrode material for electrochemical energy storage devices: Experiment and theory. *Ceram Int.* 2025; 51(14): 18886–18895.

Gaidukevic J, Aukstakojyte R, Barkauskas J, Niaura G, Murauskas T, and Pauliukaite R. A novel electrochemical sensor based on thermally reduced graphene oxide for the sensitive determination of dopamine. *Appl. Surf. Sci*. 2022; 592(1): 153257.

Ghanbari K, Moloudi M, and Bonyadi S. Modified glassy carbon electrode with silver nanoparticles/ polyaniline/reduced graphene oxide nanocomposite for the simultaneous determination of biocompounds in biological fluids. *J. Electrochem. Sci. Technol.* 2019; 10(4): 361–372.

Huang TY, Kung CW, Wei HY, Boopathi KM, Chu CW, and Ho KC. A high performance electrochemical sensor for acetaminophen based on a rGO-PEDOT nanotube composite modified electrode. *J. Mater Chem. A*. 2014; 2(20): 7229–7237.

Jackman MJ, Thomas AG, and Muryn C. Photoelectron spectroscopy study of stoichiometric and reduced anatase TiO2(101) surfaces: The effect of subsurface defects on water adsorption at near-ambient pressures. *J. Phys. Chem. C.* 2015; 119(24): 13682–13690.

Jaiswal N, Tiwari I, Foster CW, and Banks CE. Highly sensitive amperometric sensing of nitrite utilizing bulk-modified MnO2 decorated Graphene oxide nanocomposite screen-printed electrodes. *Electrochim. Acta*. 2017; 227: 255–266.

Ji T, Chen L, Schmitz M, Bao FS, and Zhu J. Hierarchical macrotube/mesopore carbon decorated with mono-dispersed Ag nanoparticles as a highly active catalyst. *Green Chem*. 2015; 17(4): 2515–2523.

Jiang L, Nelson GW, Abda J, and Foord JS. Novel Modifications to Carbon-Based Electrodes to Improve the Electrochemical Detection of Dopamine. *ACS Appl Mater Interfaces*. 2016; 8(42): 28338–28348.

Joshi A, Schuhmann W, and Nagaiah TC. Mesoporous nitrogen containing carbon materials for the simultaneous detection of ascorbic acid, dopamine and uric acid. *Sens. Actuators B Chem.* 2016; 230: 544–555.

Kenarkob M and Pourghobadi Z. Electrochemical sensor for acetaminophen based on a glassy carbon electrode modified with ZnO/Au nanoparticles on functionalized multi-walled carbon nano-tubes. *Microchem. J*. 2019; 146: 1019–1025.

Li M, Yin W, Han X, and Chang X. Hierarchical nanocomposites of polyaniline scales coated on graphene oxide sheets for enhanced supercapacitors. *J. Solid State Electrochem*. 2016; 20(7): 1941-1948.

Li S, Ma Y, Liu Y, Xin G, Wang M, Zhang Z, and

Liu Z. Electrochemical sensor based on a three dimensional nanostructured MoS 2 nanosphere-PANI/reduced graphene oxide composite for simultaneous detection of ascorbic acid, dopamine, and uric acid. *RSC Adv*. 2019; 9(6): 2997–3003.

Li YY, Kang P, Wang SQ, Liu ZG, Li YX, and Guo Z. Ag nanoparticles anchored onto porous CuO nanobelts for the ultrasensitive electrochemical detection of dopamine in human serum. *Sens.Actuators B Chem.* 2021; 327:128878.

Liu X, Fu Y, Sheng Q, and Zheng J. Au nanoparticles attached Ag@C core-shell nanocomposites for highly selective electrochemical detection of dopamine. *Microchem. J*. 2019; 146: 509–516.

Mahanthappa M, Duraisamy V, Arumugam P, and Senthil Kumar SM. Simultaneous Determination of Ascorbic Acid, Dopamine, Uric Acid, and Acetaminophen on N, P-Doped Hollow Mesoporous Carbon Nanospheres. *ACS Appl Nano Mater.* 2022; 5(12): 18417–18426.

Majidi MR and Ghaderi S. Facile fabrication and characterization of silver nanodendrimers supported by graphene nanosheets: A sensor for sensitive electrochemical determination of Imidacloprid. *J. Electroanal. Chem*. 2017; 792: 46–53.

Manivel P, Dhakshnamoorthy M, Balamurugan A, Ponpandian N, Mangalaraj D, and Viswanathan C. Conducting polyaniline-graphene oxide fibrous nanocomposites: Preparation, characterization and simultaneous electrochemical detection of ascorbic acid, dopamine and uric acid. *RSC Adv*. 2013; 3(34): 14428–14437.

Massoumi B, Fathalipour S, Massoudi A, Hassanzadeh M, and Entezami AA. Ag/polyaniline nanocomposites: Synthesize, characterization, and application to the detection of dopamine and tyrosine. *J. Appl. Polym. Sci*. 2013; 130(4): 2780–2789.

Meenakshi S, Devi S, Pandian K, Devendiran R, and Selvaraj M. Sunlight assisted synthesis of silver nanoparticles in zeolite matrix and study of its application on electrochemical detection of dopamine and uric acid in urine samples. *Mater Sci. Eng. C*. 2016; 69: 85–94.

Nayak SP, Ramamurthy SS, and Kiran Kumar JK. Green synthesis of silver nanoparticles decorated reduced graphene oxide nanocomposite as an electrocatalytic platform for the simultaneous detection of dopamine and uric acid. *Mater Chem. Phys*. 2020; 252: 123302.

Paulraj P, Umar A, Rajendran K, Manikandan A, Kumar R, Manikandan E, Kannaiyan P, Alsaiari M, Ibrahim AA, Bouropoulos N, and Baskout S. Solid-state synthesis of Ag-doped PANI nanocomposites for their end-use as an electrochemical sensor for hydrogen peroxide and dopamine. *Electrochim. Acta.* 2020; 363 :137158.

Pruneanu S, Biris AR, Pogacean F, Socaci C, Coros M, and Rosu MC. The influence of uric and ascorbic acid on the electrochemical detection of dopamine using graphene-modified electrodes. *Electrochim. Acta*. 2015; 154: 197–204.

Rahman MH, Rashed MA, Nayem NI, Rahaman MA, Ahmed J, Faisal M, Jalalh M, and Harraz FA. Nanogold-decorated reduced graphene oxide/chitosan composite for electrochemical sensing of N-acetyl-4-aminophenol. *Mater Chem. Phys*. 2024; 314: 128915.

Rashed MA, Ahmed J, Faisal M, Alsareii SA, Jalalah M, Tirth V, and Harraz FA.Surface modification of CuO nanoparticles with conducting polythiophene as a non-enzymatic amperometric sensor for sensitive and selective determination of hydrogen peroxide. *Surf. Interfaces*. 2022; 31: 101998.

Rashed MA, Faisal M, Alsaiari M, Alsareii SA, and Harraz FA. MWCNT-doped polypyrrole-carbon black modified glassy carbon electrode for efficient electrochemical sensing of nitrite ions. *Electrocatalysis*. 2021; 12(6): 650–666.

Rashed MA, Faisal M, Alsareii SA, Alsaiari M, Jalalah M, and Harraz FA. Highly sensitive and selective electrochemical sensor for detecting imidacloprid pesticide using novel silver nanoparticles/mesoporous carbon/hematite ore ternary nanocomposite. *J. Environ. Chem. Eng*. 2022; 10(6): 108364.

Sangamithirai D, Narayanan V, and Stephen A. Electrochemical detection of dopamine at poly (o-anisidine)/silver nanocomposite modified glassy carbon electrode. *Eng. J*. 2017; 9.

Shin JW, Kim KJ, Yoon J, Jo J, El-Said WA, and Choi JW. Silver nanoparticle modified electrode covered by graphene oxide for the enhanced electrochemical detection of dopamine. *Sens. Basel*. 2017; 17(12): 2771.

Wang Q, Zhang B, Lin X, and Weng W. Hybridization biosensor based on the covalent immobilization of probe DNA on chitosan-mutiwalled carbon nanotubes nanocomposite by using glutaraldehyde as an arm linker. *Sens. Actuators B Chem.* 2011; 156(2): 599–605.

Wu L, Feng L, Ren J, and Qu X. Electrochemical detection of dopamine using porphyrin-functionalized graphene. *Biosens Bioelectron.* 2012; 34(1): 57–62.

Yang L, Liu S, Zhang Q, and Li F. Simultaneous electrochemical determination of dopamine and ascorbic acid using AuNPs@polyaniline core-shell nanocomposites modified electrode. *Talanta*. 2012; 89: 136–141.

Zhang X and Zheng J. Hollow carbon sphere supported Ag nanoparticles for promoting electrocatalytic performance of dopamine sensing. *Sens. Actuators B Chem.* 2019; 290: 648–655.

Zhou X, He Y, Tao S, Wang J, Li F, and Guo Q. Selective and simultaneous sensing of ascorbic acid, dopamine and uric acid based on nitrogen-doped mesoporous carbon. *Anal. Methods*. 2020; 12(44): 5344–5352.